ANOMALOUS DELAYED LOSS OF TRAPPED D–D FUSION PRODUCTS IN TFTR

S.J. ZWEBEN, D.S. DARROW, E.D. FREDRICKSON, H.E. MYNICK
Princeton Plasma Physics Laboratory,
Princeton, New Jersey,
United States of America

ABSTRACT. A new anomalous delayed loss of D–D fusion products has been measured at the bottom of the TFTR vessel. This loss is delayed by about 0.2 s with respect to the usual prompt first orbit loss, and has a correspondingly lower energy, i.e. about half the fusion product birth energy. This loss process dominates the total fusion product loss measured 90° below the midplane for plasma currents $I \geq 1.8$ MA and major radii near $R = 2.45$ m, e.g. for recent TFTR supershots. This delayed feature can occur without large coherent MHD activity, although it can be strongly modulated by such activity. Several possible causes for this phenomenon are discussed, but no clear explanation for this delayed loss has yet been found.

1. INTRODUCTION

This paper describes measurements of an anomalous loss of partially thermalized trapped D–D fusion products to the bottom (ion ∇B direction) of TFTR. This feature is the dominant fusion product loss 90° below the midplane for plasmas with major radii of $R = 2.45$ m and plasma currents $I \geq 1.8$ MA, while for $I \leq 1.4$ MA the first orbit loss is dominant, as observed previously [1]. The relatively low energy of this loss (about half the fusion product birth energy) and its time delay of about 0.2 s (with respect to the prompt first orbit loss) imply that some unknown mechanism is causing a relatively slow leakage of fusion product ions from the plasma. Although this leakage is probably not large enough to cause a significant loss of alpha heating in future D–T tokamaks, it could potentially cause a localized alpha particle heat load which could damage the first wall.

Previous measurements of a non-first-orbit loss of trapped D–D fusion products in TFTR were made using a movable detector located 20° below the outer midplane [2]. At that location the energy of the 'anomalous' loss was near the birth energy and not significantly delayed with respect to the first orbit loss, in contrast with the results for the 90° detector described below. That loss was approximately consistent with the calculated stochastic toroidal field (TF) ripple loss [3], which causes the banana tips of high energy trapped ion orbits to diffuse vertically, leading to loss near the outer midplane where the trapped orbits first hit the wall. However, these same calculations of stochastic TF ripple loss predict a negligible TF ripple induced loss 90° below the midplane [2], and so apparently cannot explain the present anomalous delayed loss at 90°.

The delayed loss feature described below is observed in the 90° detector only for plasmas with major radii near $R = 2.45$ m, and not for plasmas with $R = 2.6$ m such as those used previously to study the diffusion of counter-passing fusion product ions [4]. The smaller plasmas consistently show this delayed loss at a plasma current $I \geq 1.4$ MA over the full range of neutral beam power up to 32 MW (in both L mode and supershot plasmas). There is usually no observable correlation of this delayed loss with MHD activity, although unusually large MHD activity does cause a coherent modulation and change in the strength of this delayed loss feature.

The basic experimental observations as described in Section 2 include data taken during the 1990 run period (Sections 2.1–2.3), data taken during the 1992 run period after a detector relocation (Section 2.4), and the effects of strong MHD activity (Section 2.5). A preliminary analysis of potentially relevant loss mechanisms is given in Section 3, and a summary and conclusions are in Section 4.

2. MEASUREMENTS OF THE ANOMALOUS DELAYED LOSS AT 90°

The escaping D–D fusion products are detected using the same experimental set-up described previously [1, 4]. The detector element is a 1×1 in^2 ZnS scintillator screen behind a pair of apertures which dis-

perse the incident MeV ions in one direction according to their gyroradius ρ (depending on their energy) and in the other direction according to their pitch angle χ (depending on their magnetic moment). The two dimensional (2-D) images of scintillator light emission are optically coupled to an intensified CCD camera for image capture and later analysis. A detector analysis code determines a (ρ,χ) grid which is used to interpret these images. For this grid the ρ co-ordinate is the centroid of the predicted scintillator impacts for an ion of gyroradius ρ (at $\chi = 90°$) and χ is the orbit's pitch angle measured locally with respect to the co-going toroidal field direction at the detector. Normally, 75% of the scintillator light emission from D–D fusion products is from the 3 MeV protons and 25% from the 1 MeV tritons [4]. Since these two ions have identical gyroradii (at birth) they are assumed to behave similarly and are treated together here as ions of a common gyroradius.

The measurements described in this section were all taken using a detector 90° below the outer midplane in the ion ∇B direction. The data of Sections 2.1–2.3 were taken during the 1990 TFTR run period when the 90° detector aperture was located about 4 cm radially outside and about 120° toroidally from the edge of the nearest 'ICRH limiter' (which are poloidal rings intended to shield the ICRH antennae). After the 1990 run a new poloidal ICRH limiter was installed only 45° toroidally from this same 90° detector, which forced a relocation of its aperture to only about 1 cm below the edge of this new limiter [5]. The data described in Section 2.4 were taken during the 1992 experimental run period with this latter configuration.

2.1. Pitch angle distributions

Typical 2-D scintillator light emission patterns observed at the 90° detector for $I = 2.0$ MA plasmas are shown in Fig. 1, where in Fig. 1(a) the plasma major radius was $R = 2.45$ m and in Fig. 1(b) it was $R = 2.6$ m. These two discharges were otherwise nearly identical, with $P = 23 \pm 1$ MW of neutral beam injection during about 3.0–4.0 s, neutron emission rates of $(1.5 \pm 0.1) \times 10^{16}$ neutrons/s between 3.3–3.4 s (the integration time for Fig. 1), and $B = 4.9$ T on axis. The contours of Fig. 1 show the raw 2-D images at nine levels from 10–90% of their peak signals. The light emission patterns for the $R = 2.6$ m in Fig. 1(b) are nearly identical to those analysed previously [4], which were consistent with the first orbit loss model without any anomalous loss.

However, the (ρ,χ) pattern for the $R = 2.45$ m case in Fig. 1(a) was significantly different, with a peak signal located at a significantly higher χ and a lower ρ than for the $R = 2.6$ m case. The pitch angle distributions for these same two discharges are directly compared in Fig. 2(a), after averaging over gyroradius centroid positions $\rho = 2$–11 cm for 3.3–3.4 s. For the $R = 2.6$ m case the peak was at $\chi \approx 63°$, which is similar to the previous $R = 2.6$ m case, and agreed

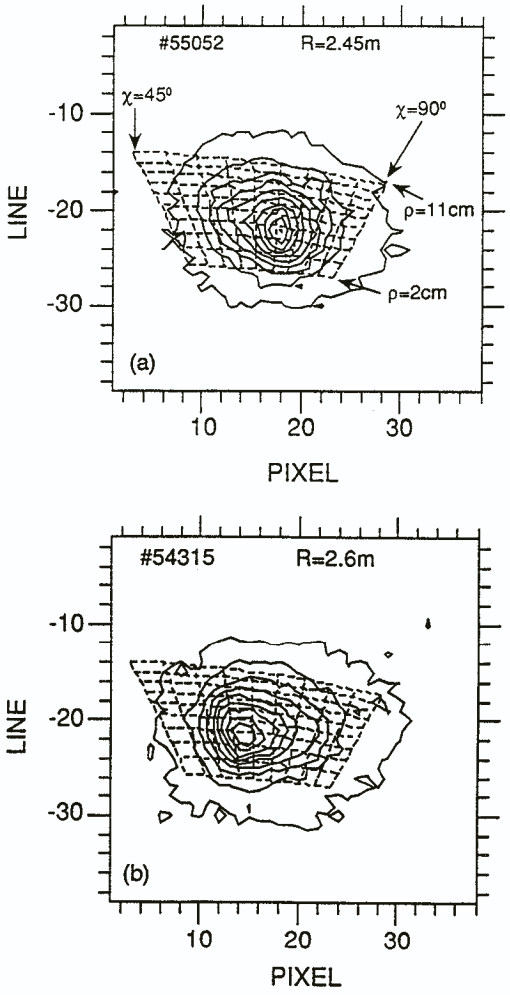

FIG. 1. Contour plots of the pitch angle against gyroradius pattern of loss to the 90° detector for two similar discharges, one at (a) R = 2.45 m (#55 052) and the other at (b) R = *2.6 m (#54 315). For both discharges the plasma current was* I = *2.0 MA, the beam power was* P = *22–23 MW and the data were taken during the time 3.3–3.4 s. The anomalous loss feature visible for case (a) occurs at an unexpectedly high pitch angle* $\chi \approx 70°$ *and low gyroradius* $\rho \approx 4$–*5 cm.*

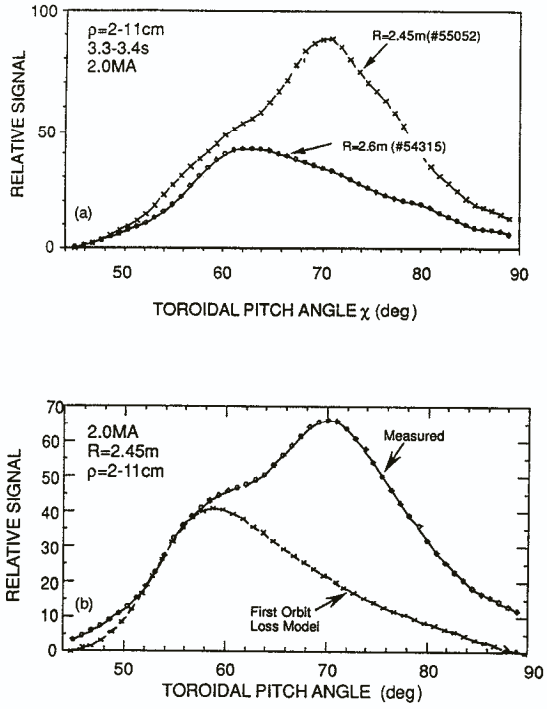

FIG. 2. Pitch angle distributions for the two I = *2.0 MA cases in Fig. 1. In (a) is a direct comparison between the shapes of the pitch angle distributions for the* R = *2.45 m and* R = *2.6 m cases, showing the anomalous peak at* $\chi \approx 70°$ *for the* R = *2.45 m case. In (b) is a comparison between the measured pitch distribution for the* R = *2.45 m case and the calculated first orbit loss distribution (normalized to the data at* $\chi \approx 55°$*), which shows that the measured peak at* $\chi \approx 70°$ *is not predicted by the first orbit loss model.*

with the first orbit model to within 2° [4]. However, for the $R = 2.45$ m case the first orbit model predicts the peak to be at $\chi \approx 59°$, as illustrated in Fig. 2(b), clearly disagreeing with the measured peak at $\chi \approx 70°$. Note that the first orbit model curve in Fig. 2(b) was normalized to the data at $\chi \approx 55°$, suggesting that the measured χ distribution at $R = 2.45$ m does contain a first orbit loss component somewhat smaller than the anomalous component, which peaks near $\chi \approx 70°$.

This apparent two peak structure of the pitch angle distributions for $R = 2.45$ m plasmas can be seen more clearly in the scan of plasma current from $I = 0.8$–2.5 MA shown in Fig. 3. For plasma currents $I \leq 1.4$ MA the pitch distributions agree well with those expected for first orbit loss [1], while for currents $I \geq 1.6$ MA the second peak at $\chi \approx 70°$ begins to appear and eventually dominates the signal at $I \geq 1.8$ MA. Note that only the shapes of the pitch angle distributions are shown here, while the relative magnitudes versus current are discussed in Section 2.3. For a similar current scan at $R = 2.6$ m the pitch distributions showed a close agreement with the first orbit model over $I = 0.6$–2.0 MA [4], including an expected *decrease* in the peak pitch angle with increasing current.

For the $I = 2.0$ MA case the peak pitch angle of $\chi \approx 70°$ with respect to the local toroidal field corresponds to a 74° pitch angle with respect to the total magnetic field at the detector. Thus, the anomalous loss feature corresponds to a rather deeply trapped ion with its banana tip near the major radius of the plasma centre, i.e. not near the passing–trapped boundary, which is at $\chi \approx 55°$ for 3 MeV protons lost at this location (see Section 3.1 for a discussion of the orbit trajectories). Although stochastic TF ripple diffusion is expected to involve orbits with banana tips below the plasma centre [2], calculations of the poloidal distribution of this loss mechanism strongly suggest that it would be highly localized near the outer midplane. Therefore, this high pitch anomaly is not likely to be due to TF ripple loss (see also Section 3.4.2).

These pitch angle data were integrated over the period from about 0.5–1.0 s after the start of NBI, during which time the distributions were approximately constant. However, the pitch distributions were significantly different earlier during the NBI pulse and after the NBI pulse ended, as shown in Fig. 4(a) for a $I = 1.8$ MA discharge (shown earlier in Fig. 3), with 7.5 MW of NBI from 3.0–4.0 s. About 0.1 s after the start of NBI the anomalous loss peak near $\chi \approx 70°$ was relatively small compared with the first orbit peak near $\chi \approx 60°$, while about 0.1 s after the NBI was switched off (while the neutron source rate was falling) the anomalous loss peak was relatively larger compared with the first orbit peak. The shapes of these distributions became constant about 0.3–0.4 s after the start of NBI, as indicated by the time dependence of the gyroradius peak location in Fig. 4(b), plotted along with the $I = 2.0$ MA case shown in Fig. 2.

Another characteristic of the high current pitch angle distributions at $R = 2.45$ m was a tendency for the anomalous loss feature to increase with NBI power (in the steady state), when compared with the first orbit loss feature. This is illustrated in Fig. 5 for three $I = 2.0$ MA cases at $P = 7.5$, 12 and 25 MW. These curves are normalized together at $\chi \approx 55°$ (near the first orbit loss region), showing how the anomalous feature increases with NBI power. This suggests that the anomalous feature depends upon some plasma property which changes with NBI power.

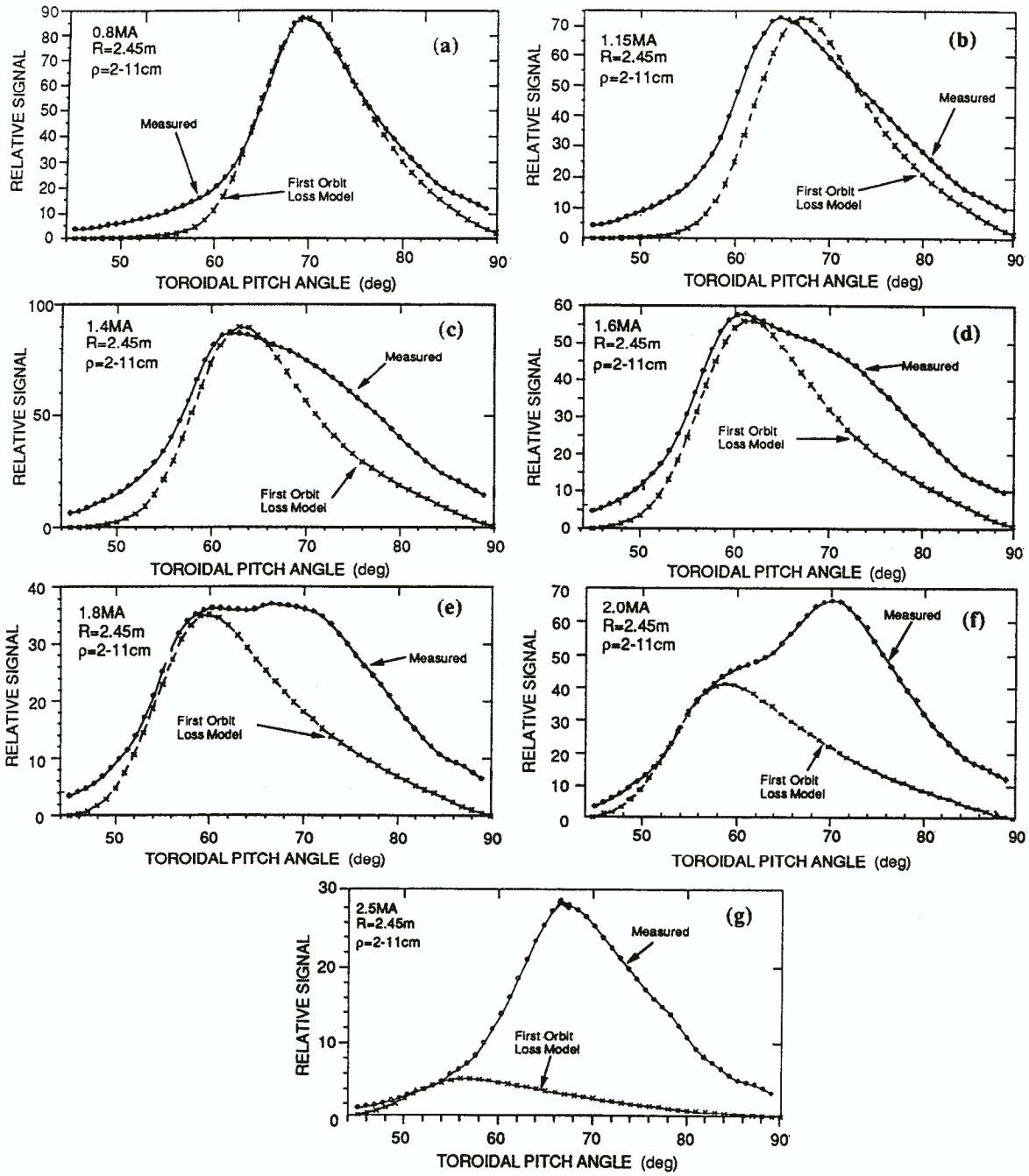

FIG. 3. Measured pitch angle distributions and calculated first orbit loss distributions for R = *2.45 m plasmas as functions of plasma current. For currents* I ≤ *1.4 MA the measured distributions agree fairly well with the first orbit model, while for currents* I ≥ *2 MA the anomalous loss feature at* $\chi \approx 70°$ *dominates. These measured pitch distributions were taken during the steady state part of NBI (typically 3.5–4.0 s in a 3.0–4.0 s NBI pulse), and the model curves for* I ≥ *1.8 MA were normalized to the data at* $\chi \approx 55°$. *Note that the vertical scales are not comparable from one current to the next (see Fig. 8).*

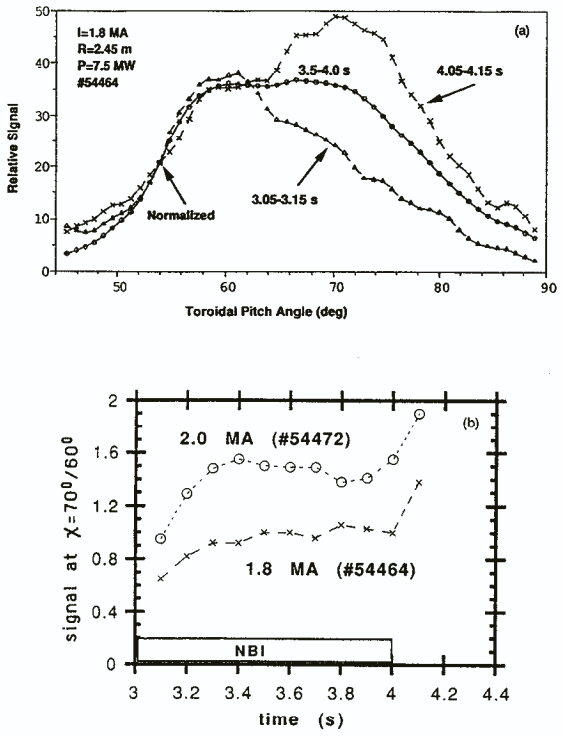

FIG. 4. Part (a) shows the pitch angle distributions (integrated over ρ = 2–11 cm) just after the start of NBI and just after the end of NBI for the I = *1.8 MA,* R = *2.45 m discharge shown in Fig. 3(e) (#54 464). Just after the start of NBI the anomalous loss feature at* $\chi \approx 70°$ *is relatively smaller (compared with the first orbit loss feature) than it is during the steady state phase at about 3.5–4.0 s and just after NBI it is relatively larger. The ratio of the signal at* $\chi \approx 70°$ *to the signal at* $\chi \approx 60°$ *is plotted in part (b) for this case, and also for the I = 2 MA case of Fig. 2, showing that the shapes of these distributions become constant about 0.4 s after the start of NBI. This behaviour implies that the anomalous feature is a delayed loss process.*

2.2. Gyroradius distributions

The present detector uses the geometrical dispersion of the MeV ion orbits through the aperture pair to determine the gyroradius ρ, which is defined here as the gyroradius which the incident ion would have had at a 90° pitch angle. As discussed previously [4], there is a considerable instrumental broadening in this detector due to the finite aperture heights, which spreads orbits of a given gyroradius across the ρ dimension of the scintillator plane. Although the measured distributions will be displayed on a grid which represents the *centroid* locations of the ion impacts of various gyroradii (see Fig. 1), the measurements should actually be compared with the outputs of a detector simulation code which includes the instrumental resolution.

Figure 6 shows a comparison between the ρ distributions for an $I = 2.0$ MA discharge (dominated by the anomalous loss feature) and an $I = 0.8$ MA discharge (dominated by first orbit loss), both cases having $R = 2.45$ m at the same toroidal field ($B = 4.8$ T at $R = 2.45$ m), again from the current scan in Fig. 3. Note that the peaks of the corresponding pitch angle distributions are both near $\chi \approx 70°$, which makes the inference of their relative gyroradius distribution (averaged over $\chi \approx 45$–$85°$) less sensitive to possible systematic errors in the (ρ,χ) grid. Also shown in Fig. 6 are calculated particle impact distributions based on assumed incident gyroradii of 4, 5 and 6 cm. The $I = 0.8$ MA data fit the curve for $\rho = 6$ cm, roughly consistent with the first orbit loss expected at $\rho = 5.5$ cm (for 3 MeV protons or 1 MeV tritons). However, the $I = 2.0$ MA curve peaks at a significantly lower gyroradius near $\rho = 4.5 \pm 0.5$ cm. This implies that the average energy of the fusion product loss for this case, normalized to the energy for the prompt first orbit loss E_0, is roughly

$$E/E_0 \approx [(4.5 \pm 0.5)/6]^2 \approx 55 \pm 15\%$$

i.e. corresponding to protons of about 1.5 MeV instead of the 3 MeV expected for the proton birth energy.

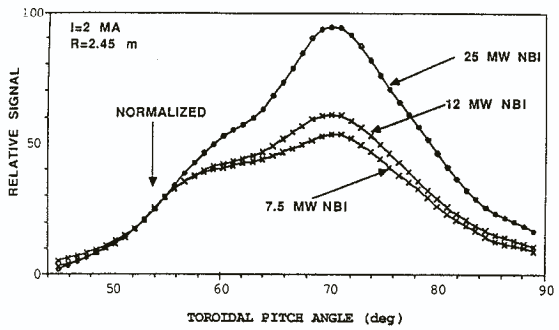

FIG. 5. Pitch angle distributions for plasmas with varying NBI power at R = *2.45 m and I = 2.0 MA, taken during the steady state part of the discharge and normalized at their first orbit regions at* $\chi \approx 55°$. *The discharge with the lowest NBI power of 7.5 MW (#54 468) had the smallest anomalous feature, while those with 12 and 25 MW (#54 472 and 55 050, respectively) had a larger anomalous loss peak, relative to the first orbit feature at lower pitch angles. The total MeV ion loss (normalized by the neutron rate) increased by about 40% over this power range.*

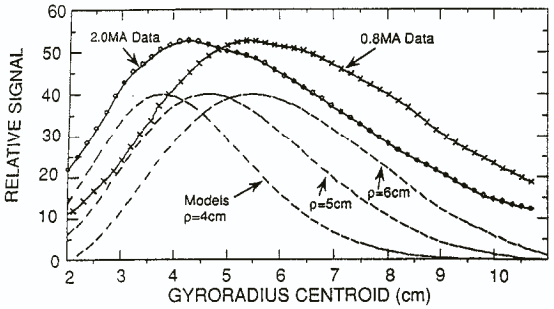

FIG. 6. Gyroradius distributions for I = *0.8 MA and* I = *2.0 MA plasmas (integrated over* $\chi \approx 45$–$90°$ *during 3.5–4.0 s) compared with model calculations for assumed gyroradii of* ρ = *4, 5 and 6 cm. The* I = *0.8 MA case fits fairly well the expected* ρ = *5.5 cm for prompt first orbit loss, while for the* I = *2.0 MA case the total loss is best fitted by an assumed* $\rho \approx$ *4–5 cm, implying an average loss energy of* $E/E_0 \approx$ *0.5–0.6 compared with the birth energy. The broadening due to instrumental effects causes the calculated distributions to be spread over a range of gyroradius centroid locations.*

The large instrumental broadening (as shown by the model curves) and various systematic uncertainties [4] do not allow a direct decomposition of the measured distribution at I = 2.0 MA into prompt and delayed energy components, but since the prompt loss should be near the birth energy, it is likely that the anomalous loss had an energy somewhat below half the birth energy.

This trend for the anomalous loss feature to have a lower energy than the first orbit loss can also be seen in Fig. 7, which shows the gyroradius distributions for three times during the same I = 1.8 MA discharge shown in Fig. 4. About 0.1 s after the start of NBI the gyroradius distribution is close to that for first orbit loss at 0.8 MA (Fig. 6), peaking near the ρ = 6 cm centroid, i.e. appreciably below the peak location measured during the steady state phase of about 3.5–4.0 s. About 0.1 s after NBI ends, the distribution shifts to an even lower gyroradius, peaking just below the ρ = 4 cm centroid. The shape of the gyroradius distribution attains its steady state shape about 0.3 s after the start of NBI.

Therefore, both the time and energy dependences of the anomalous loss are consistent with a time delay between the ion's birth and its loss. This estimated time delay of about 0.2 $\pm$ 0.1 s is approximately the same as the time required for classical collisions to slow 3 MeV protons down to 1.5 MeV in these plasmas with $T_e(0) \approx$ 7–8 keV and $n_e(0) \approx$ (5–6) $\times 10^{13}$ cm^{-3}, implying that these ions are thermalizing classically while diffusing anomalously. This is qualitatively similar to the results from triton burnup measurements in TFTR [6], which implied a classical slowing down but anomalous diffusion of 1 MeV tritons.

2.3. Magnitude of the anomalous MeV ion loss

The total MeV ion loss to the 90° detector can be estimated from the total light emission within the (ρ,χ) grid shown in Fig. 1, averaged during the steady state phase of NBI (typically 3.5–4.0 s), and normalized by the neutron rate during that time. The relative MeV ion loss signal obtained in this way for a set of R = 2.45 m plasmas is plotted versus plasma current in Fig. 8. These discharges were chosen to have moderate NBI power (P = 6–20 MW, increasing with current) without large coherent MHD activity in the MeV ion signals (see Section 2.5). Some of their pitch angle distributions were shown in Fig. 3.

Note that this analysis procedure does not explicitly correct for the dependence of the light emission on the ion energy. However, this correction should be relatively small, since the scintillator light output for D–D fusion products is relatively insensitive to the ion energy in this range, e.g. the signal from protons and tritons with half their birth energy (as inferred in Section 2.2) would be about 0.7 times the signal for birth energy ions [4]. Correction for this effect would imply that the anomalous particle flux (ions/s) would be slightly larger than that indicated below.

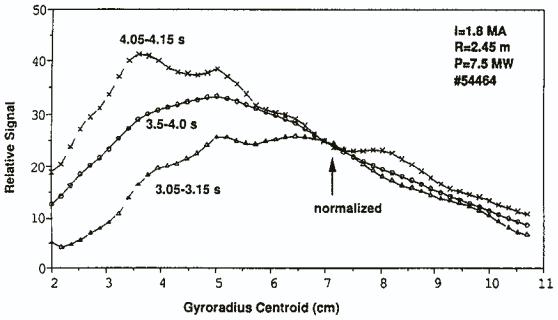

FIG. 7. Gyroradius distributions (integrated over $\chi \approx 45$–$90°$*) versus time during the same* I = *1.8 MA discharge as for Fig. 4. Just after the start of NBI the gyroradius distribution is similar to that for the first orbit loss at 0.8 MA shown in Fig. 6, while just after NBI ends the peak of the gyroradius distribution occurs at an even lower value of* ρ *than during the period from about 3.5–4.0 s. This confirms the delayed nature of this loss.*

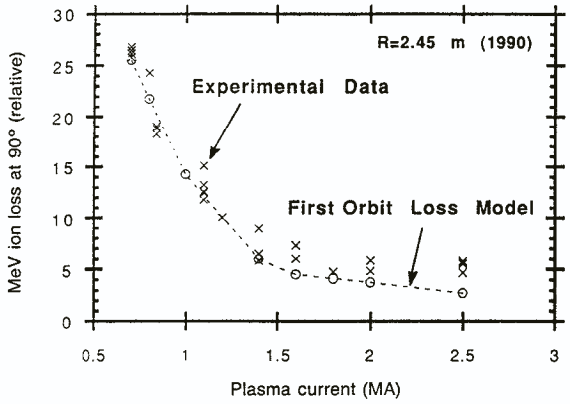

FIG. 8. Total MeV ion signal versus plasma current for discharges with R = *2.45 m (in the range #53 360–55 362). The ordinate is the total scintillator light output during the period from 3.5–4.0 s during NBI, normalized by the total neutron rate during that time. The relative loss between* I = *0.7–1.4 MA follows the first orbit model curve fairly well (as calculated for discharges in this sequence), but the measured loss between* I = *1.4 and 2.5 MA decreases less than expected from the first orbit loss model.*

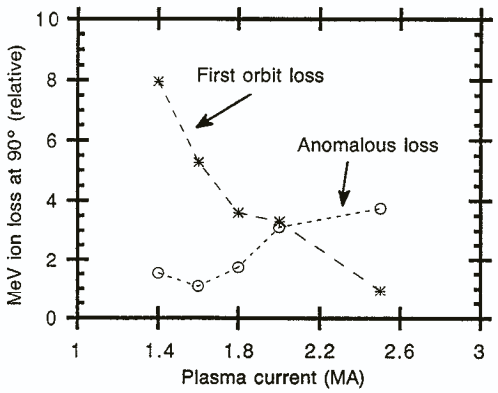

FIG. 9. Approximate decomposition of the MeV ion pitch angle distributions of Fig. 3 into a 'first orbit' part (with the shape of the calculated first orbit loss distribution normalized to the data at $\chi \approx 55°$*) and an anomalous part (the remaining signal centred near* $\chi \approx 70°$*). Over the range* I = *1.4–2.0 MA the anomalous loss signal appears to increase by about a factor of two, while the first orbit part decreases by a factor of about 2.5. There is also a systematic change in the anomalous loss component with NBI power (not shown here), and a possibility that the data at* I = *2.5 MA are affected by shadowing from the ICRH limiter.*

Figure 8 shows that the relative MeV ion loss decreased by a factor of about five with increasing current over the range I = 0.7–2.5 MA, while the expected first orbit loss decreases by about a factor of ten over this same range. When the first orbit loss calculation is normalized to the data at I = 0.7 MA (where the first orbit loss is expected to dominate), then the total loss at $I \geq 1.8$ MA appears to be not more than a factor of two above that expected from the first orbit model. However, there are uncertainties of at least ±50% in the calculated first orbit loss at $I \geq 1.8$ MA (with respect to that at 0.7 MA), due to uncertainty in the neutron source and plasma current profiles [4], which make it difficult to draw quantitative conclusions concerning the scaling of the anomalous loss versus current from this figure alone.

Another approach to isolating the anomalous loss component is to decompose the pitch angle distributions of Fig. 3 into a 'first orbit' part which fits the calculated first orbit loss pitch angle distribution, and a residual part which represents the anomalous loss peaked near $\chi \approx 70°$. Figure 9 shows the results of such an analysis for the I = 1.4–2.5 MA cases in Fig. 3. The anomalous loss component (in the same units as those in Fig. 8) appears to increase by about a factor of two between I = 1.4 and 2.0 MA, while the first orbit loss component apparently decreases by a factor of 2.5 over the same range. The surprisingly low first orbit loss component at I = 2.5 MA may be due to the effect of the ICRH limiter, which comes close to intercepting birth energy orbits entering the detector at this location with low pitch angles at R = 2.45 m (see Section 3.1).

The approximate dependence of the anomalous loss signal on the neutral beam power in the narrow current range I = 1.85–2.0 MA is shown in Fig. 10. There, the

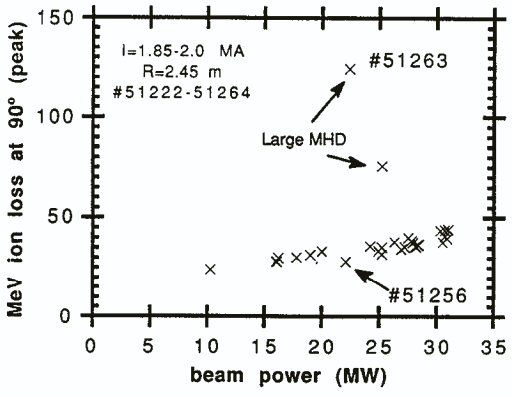

FIG. 10. The effect of NBI power on the relative MeV ion loss signal measured near the peak of the anomalous loss feature for a set of I = *1.85–2.0 MA discharges (averaged over 3.5–4.0 s in discharges with NBI from 3–4 s). The neutron normalized peak loss increases slowly with NBI power, which is not expected for first orbit loss, while the pitch distributions change as shown in Fig. 5.*

MeV ion signal at the peak of the anomalous loss feature (including a contribution of about 30% from first orbit loss) is plotted versus NBI power over the range P = 10–31 MW (after normalizing by the neutron rate during the integration time of 3.5–4.0 s in discharges with NBI from 3–4 s). The peak loss signal increased by nearly a factor of two over this power range, while the location of the peak remains nearly constant (ρ = 4.2 ± 0.5 cm and χ = 68 ± 2°). Note that the first orbit part of this peak loss signal may increase by up to about 50% with NBI owing to the Shafranov shift and broadened source profiles, but this would only contribute about 10–20% to this factor-of-two change. The total loss rate (averaged over ρ = 2–11 cm and χ = 45–90°) increased similarly with NBI power in high current discharges without large MHD [7]. The discharges with 'large MHD' are discussed in Section 2.5.

2.4. Measurements after relocation of the 90° detector

After the data of Sections 2.1–2.3 were taken, the 90° detector was moved radially inward 3.3 cm to avoid the shadowing effect of a new poloidal limiter installed in 1991. The scintillator material was also changed from ZnS(Ag) (blue) to ZnS(Cu) (green), and an improved carbon composite heat shield was added [5]. Most features of the D–D fusion product loss were similar before and after the change; in particular, the (ρ,χ) patterns and time dependences for plasmas with R = 2.6 m (which did not show any anomalous

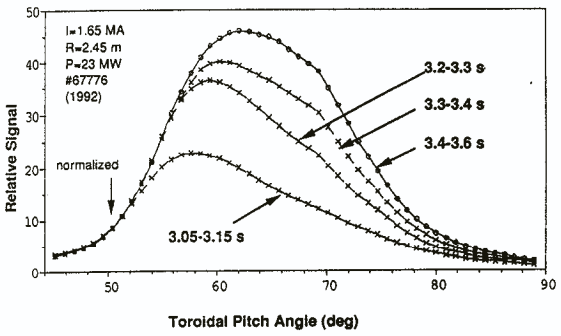

FIG. 11. Time dependence of the pitch angle distribution measured for a typical R = 2.45 m plasma during the 1992 run period (averaged over $\rho \approx$ 2–11 cm). The pitch angle distribution is consistent with the expected first orbit loss distribution up to about 0.2 s after NBI starts, but after about 0.3–0.4 s the distributions show an anomalous delayed loss feature near $\chi \approx$ 70°, qualitatively similar to that seen during the 1990 run period.

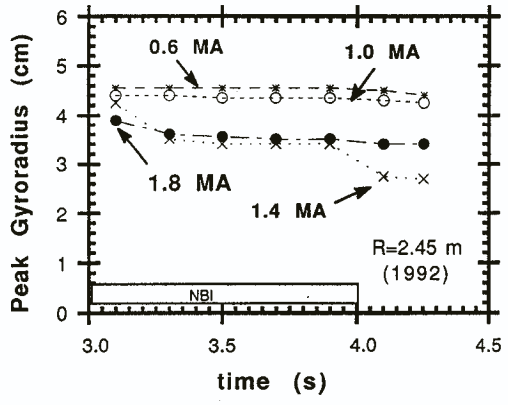

FIG. 12. Peak of the gyroradius distribution (in terms of its centroid location) versus time (averaged over χ = 45–90°) for a series of R = 2.45 m discharges during the 1992 run period. The gyroradius distribution remains approximately constant in time for I ≤ 1.0 MA as expected for first orbit loss, but for I ≥ 1.4 MA there is a decrease in the peak gyroradius past about 0.2 s after NBI, which is at least qualitatively similar to the gyroradius distributions seen in the 1990 run (Fig. 6).

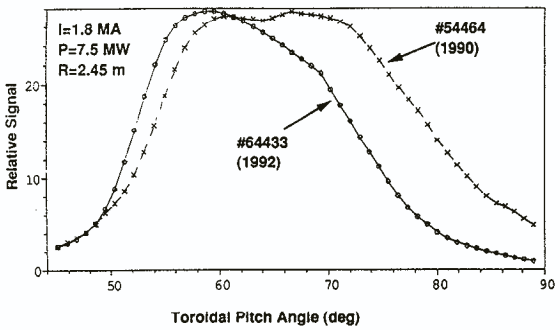

FIG. 13. Comparison of the pitch angle distributions measured by the 90° detector for 1990 and 1992 discharges, both at 1.8 MA, R = 2.45 m and P = 7.5 MW (averaged over $\rho \approx$ 2–11 cm during 3.5–4.0 s). There is a significant difference in the shape of the two distributions, which is attributed to relatively more anomalous delayed loss at low pitch angles (χ = 55–65°) in the 1992 run, after a repositioning of the 90° detector aperture. These two curves are normalized to each other at χ = 60°.

delayed loss) were nearly the same, as were those for R = 2.45 m plasmas at I < 1.4 MA. The absolute flux of D–D fusion products inferred for these cases was also the same in both years (to within a factor of two uncertainty in the cross-calibration).

The *qualitative* features of the anomalous delayed loss for R = 2.45 m plasmas with $I \geq$ 1.4 MA in 1992 were also similar to the earlier data, as illustrated by Figs 11 and 12. The pitch angle distributions shown

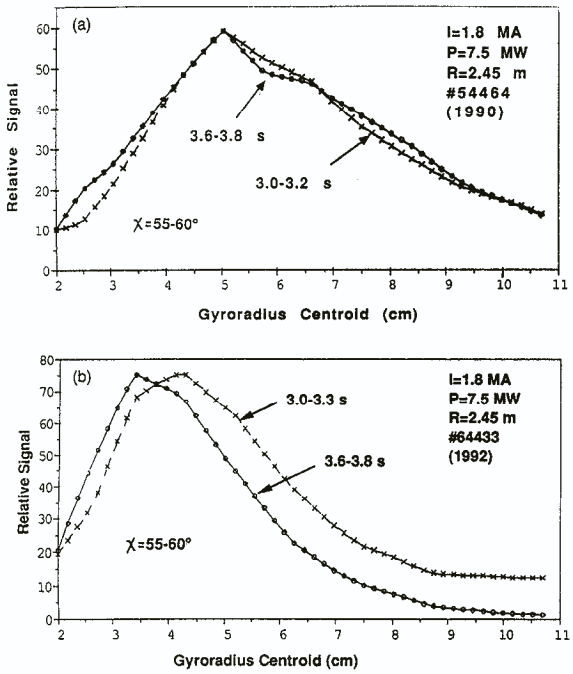

FIG. 14. Comparison of the gyroradius distributions measured by the 90° detector within the pitch angle region χ = 55–65° for the (a) 1990 and (b) 1992 discharges shown in Fig. 13. There is a significant decrease in the peak of the gyroradius distribution versus time in this range for the 1992 data, but not for the 1990 data, indicating that there is a significant anomalous delayed loss at these low pitch angles in the 1992 data.

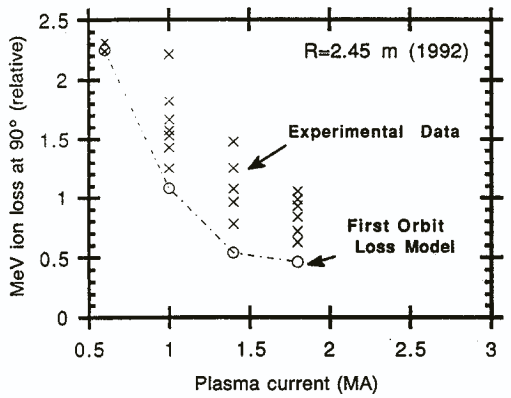

FIG. 15. Total MeV ion loss signal versus plasma current for discharges with R = 2.45 m for the 1992 run (in the range #64 429–64 462), similar to the plot for the 1990 data in Fig. 8. The relative loss between I = 0.6–1.8 MeV does not decrease as much as expected from the first orbit model (as calculated for discharges in this sequence), and appears to decrease less than the corresponding data from 1990.

in Fig. 11 had a shape close to that predicted for first orbit loss up to about 0.2 s after NBI, but then evolved over the next ≈0.3 s to a shape with an additional anomalous loss near $\chi \approx 70°$, i.e. similar to the behaviour shown in Figs 2 and 4. Over this same time interval the gyroradius peak decreased from about 4.5 cm to about 3.6 cm, as shown in Fig. 12, implying an average energy of the decrease to $E/E_0 \approx 0.6$, i.e. again similar to the 1990 results in Fig. 6.

On the other hand, the detailed shapes of the pitch angle distributions at $I \geq 1.4$ MA were different between 1992 and 1990, as illustrated by Fig. 13 for two R = 2.45 m, I = 1.8 MA discharges at $P \approx 7.5$ MW. The two peak structure which was evident in Figs 2 and 3 was not so clear in the 1992 data, which instead had a relatively larger feature near the expected first orbit loss peak at $\chi \approx 55$–60°. In principle, this could be due either to a decrease in the anomalous delayed loss near $\chi \approx 70°$, or to an increase in the anomalous delayed loss near $\chi \approx 55$–60°. The latter is strongly suggested by the results of Fig. 14, which show a decrease in the average loss energy versus time in the region $\chi \approx 55$–60° in the 1992 data, but not in the 1990 data (which showed delayed loss only near $\chi \approx 70°$). The implication is that after its repositioning the 90° detector collected *more* anomalous delayed loss at low pitch angles near $\chi \approx 55$–60° than it had previously, presumably because these ions had not reached the aperture of the detector in the 1990 run (see Section 3.1).

Further evidence for an increase in the delayed loss after the detector relocation was seen in the dependence of the total loss on plasma current shown for the 1992 data in Fig. 15. When the total loss was normalized to the data at the lowest current, as it was for the 1990 data in Fig. 8, the resulting loss at I = 1.8 MA was about a factor-of-two above the expected first orbit loss, i.e. higher than the corresponding anomaly in the data from 1990 in Fig. 8. Note that the scatter in the I = 1.8 MA data in Fig. 15 was mainly due to a systematic increase in the anomalous delayed loss with NBI power, similar to that shown in Fig. 10, and not due to MHD activity (this 1992 data was taken at low NBI powers of P = 2.5–12 MW).

The time dependences of the total D–D fusion product loss for typical moderate power R = 2.45 m discharges from 1992 are shown in Fig. 16. In these cases the total loss was monitored by a fast photomultiplier (PM) tube, which was not available in 1990, and the total loss signal was normalized to the neutron rate at 3.1 ± 0.5 s, i.e. 0.1 s after NBI. For the I = 0.6 and 1.0 MA cases there was a close proportionality between the MeV ion loss signal and the

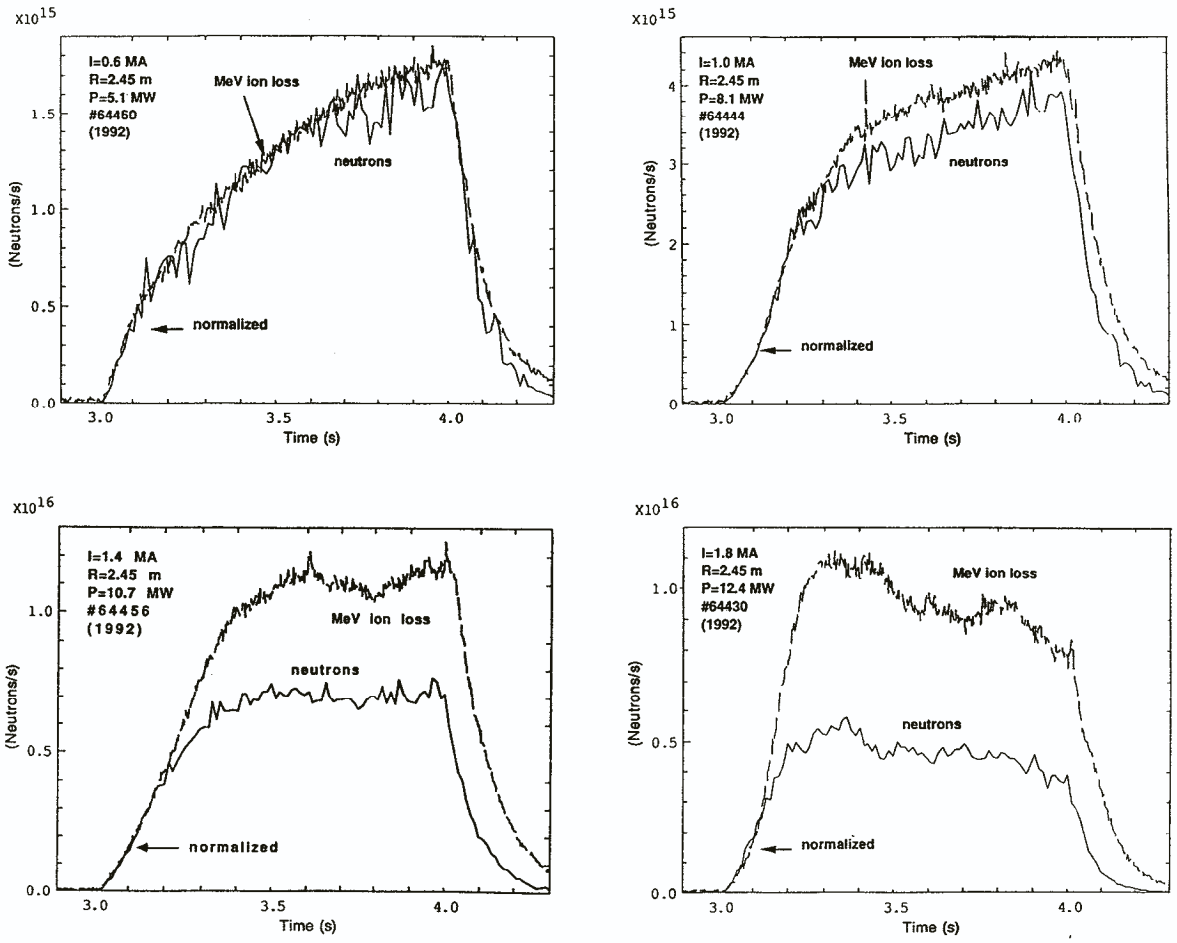

FIG. 16. Time dependences of the total loss signal from the 90° detector for R = *2.45 m discharges from the 1992 run (measured using a fast photomultiplier detector). For* I = *0.6 and 1.0 MA the measured loss is proportional to the neutron rate, while for* I = *1.4 and 1.8 MA there is a significant delayed loss component starting at about 0.2 s after NBI, and lasting up to about 0.3 s after NBI ends. For each current the MeV ion loss is normalized to the neutron rate at 3.1 ± 0.05 s.*

neutron rate, as expected for prompt first orbit loss. For the higher current cases there was a delayed loss starting at about 0.15 s after NBI, increasing to about a factor-of-two above the expected prompt loss rate after about 0.4 s, and persisting up to about 0.3 s after the end of NBI.

Examination of the 1992 data from the fast PM monitor also showed no consistent fluctuations in the range from about 1 Hz $< f <$ 20 kHz during the anomalous delayed loss, except during large MHD activity (generally at high NBI powers). For $R = 2.6$ m discharges in the 1992 run there was a close proportionality between the MeV ion loss and the neutron rate versus time for all plasma currents up to 1.8 MA (up to at least $P \approx 15$ MW), i.e. similar to the results of 1990.

2.5. Effects of MHD activity on the anomalous loss feature

For nearly all beam heated plasmas with $I \geq 1.4$ MA at $R = 2.45$ m the anomalous delayed loss feature in the 90° detector remained approximately invariant after about 0.4 s past the start of NBI, and persisted very reproducibly over the 1990–1992 run periods. The exceptions to this reproducible behaviour all seemed to

occur during discharges with strong MHD activity, when both the magnitude and the (ρ,χ) structure of the anomalous loss feature could vary substantially.

The most common effect of large MHD activity was to increase the loss rate within the region near the peak of the anomalous loss feature. The time dependence of the loss within this region ($\rho \approx$ 3–4 cm, $\chi \approx$ 65–70°) is shown in Fig. 17(a) for a pair of discharges taken from Fig. 10, one of which had 'large MHD'. The peak signal increased by over a factor of ten in the MHD active discharge (#51 263) compared with the comparison case (#51 256), while the neutron rate decreased by only about 30%. The shot with 'large MHD' had slow ($\approx$0.1–0.3 kHz) $m = 2$, $n = 1$ activity after 3.25 s at an unusually large level of $\tilde{B}_r/B_T \approx 5 \times 10^{-4}$ (estimated near the $q = 2$ surface), along with high n kink activity, while the comparison shot had a few sawteeth along with $m = n = 1$ fishbone activity, as did most of the other discharges of Fig. 10. The shot with 'large MHD' in Fig. 17 had a variety of (ρ,χ) loss patterns during the MHD activity, most often with an unusually large high χ feature at an unusually low ρ (e.g. as shown at 3.56 s), as if the MHD activity was increasing the delayed loss process, although at times the peak loss moved to near the passing–trapped boundary (e.g. at 3.89 s). The shot with sawteeth and fishbone activity had a relatively normal (ρ,χ) distribution for this current and power. Note that this increased loss associated with MHD activity could persist for over 0.5 s, i.e. longer than a 3 MeV proton slowing down time.

As shown in Fig. 17(a), this increased loss associated with large MHD activity often fluctuated from frame to frame as viewed by the relatively slow video

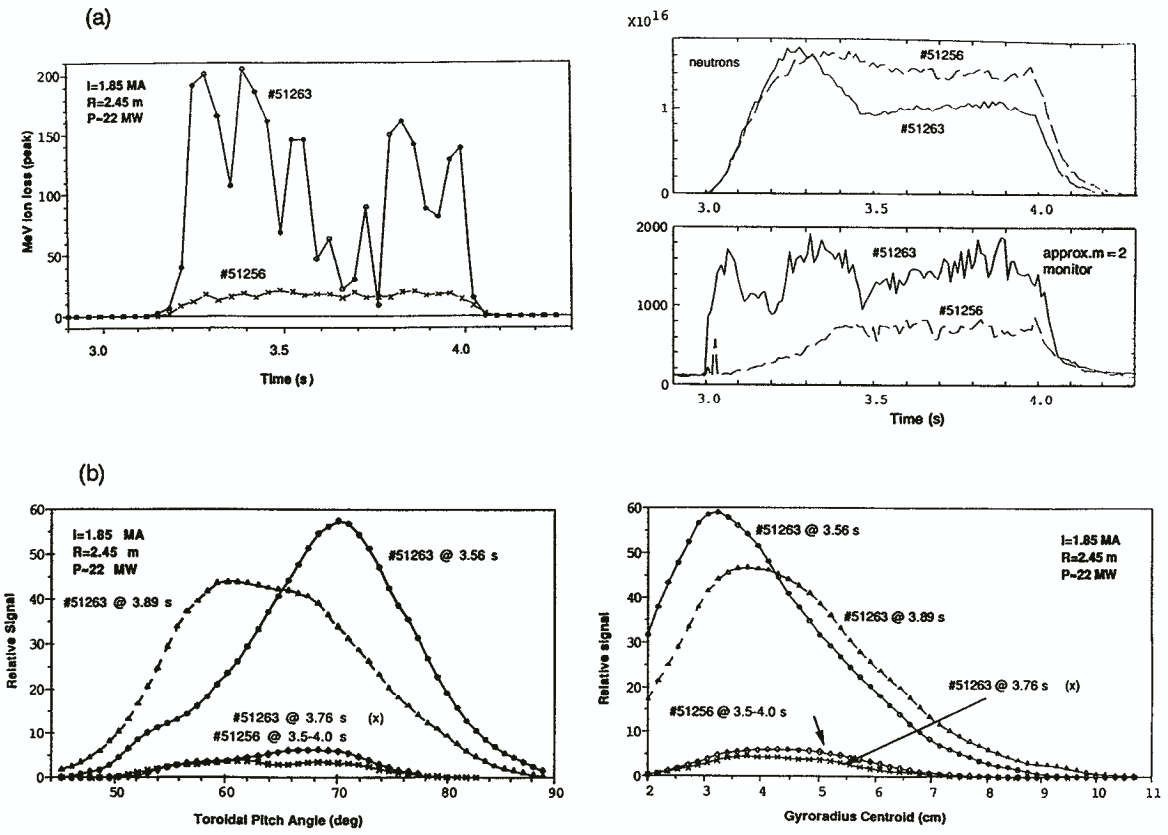

FIG. 17. Time dependences of the MeV ion loss signals for two different discharges (from the 1990 run) with R = *2.45 m,* I = *1.85 MA and* P ≈ *22 MW. One of these has large* m = *2,* n = *1 MHD activity (#51 263), while the other does not (#51 256). During the MHD activity the instantaneous MeV ion loss can increase by over a factor of ten, while the neutron rate is reduced by only <30%. The pitch angle and gyroradius distributions vary considerably versus time during the discharge with MHD activity, sometimes showing a large increase in the delayed loss feature at* $\chi \approx 70°$ *and an unusually low gyroradius distribution peaked at* $\rho \approx 3$ *cm (e.g. at 3.56 s).*

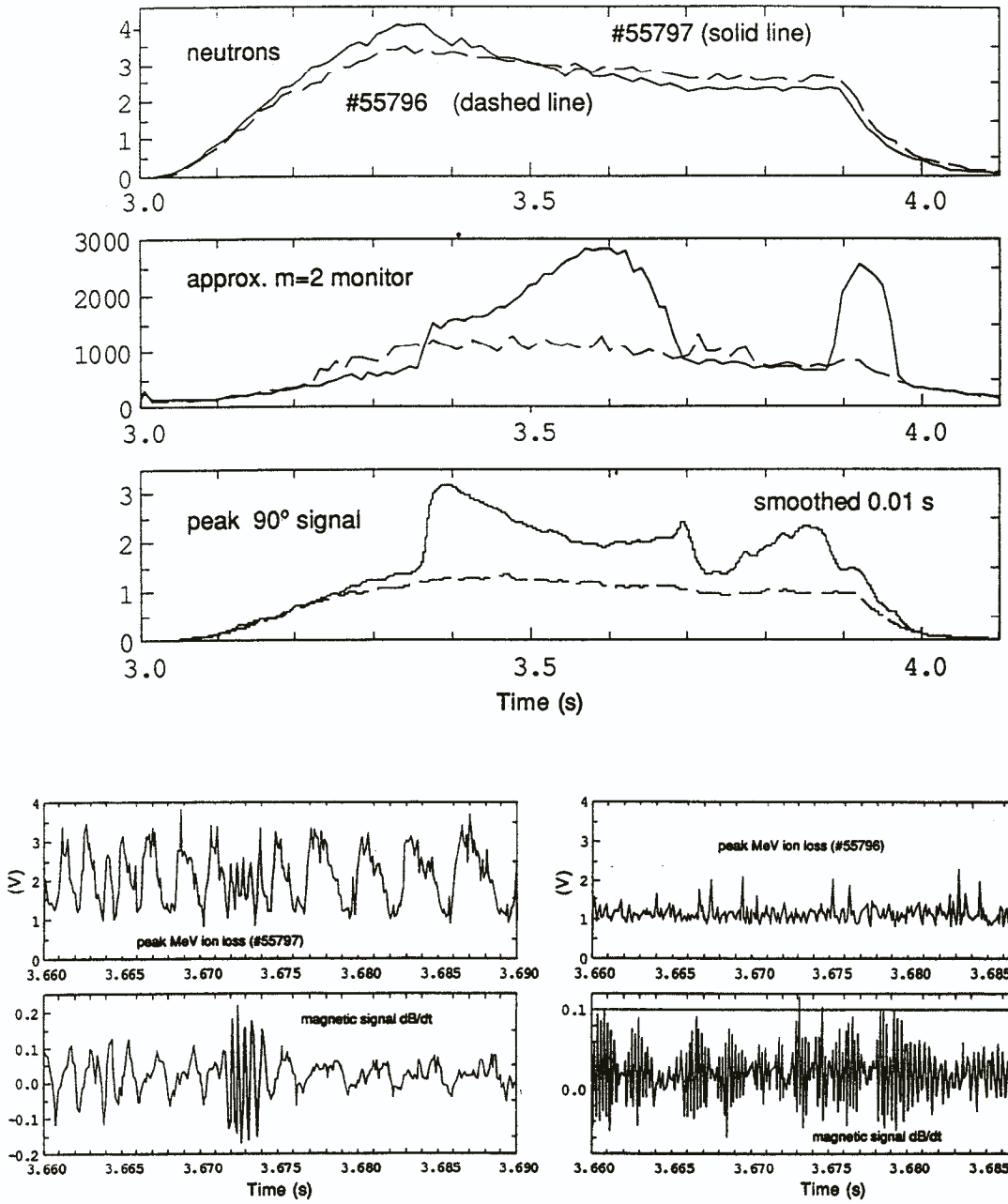

FIG. 18. Time dependences of the MeV ion loss signal near the peak of the anomalous delayed loss feature for a discharge with large low frequency MHD activity (#55797), compared with a discharge with much smaller MHD activity (#55796). These discharges had similar neutron rates, but different low frequency MHD activity and different MeV ion loss at 90°, as shown in the top part of the figure. The peak MeV ion loss signal in #55797 increases by about a factor of two with the onset of the MHD activity at about 3.35 s and fluctuates in phase with the ≈0.5 kHz magnetic loop signals, while it does not appreciably increase or fluctuate with the smaller ≈5 kHz fluctuations in #55796 (note that the magnetic signals shown are proportional to dB/dt). This fusion product loss signal comes from a PM tube monitoring the peak emission region with a frequency response of up to about 20 kHz.

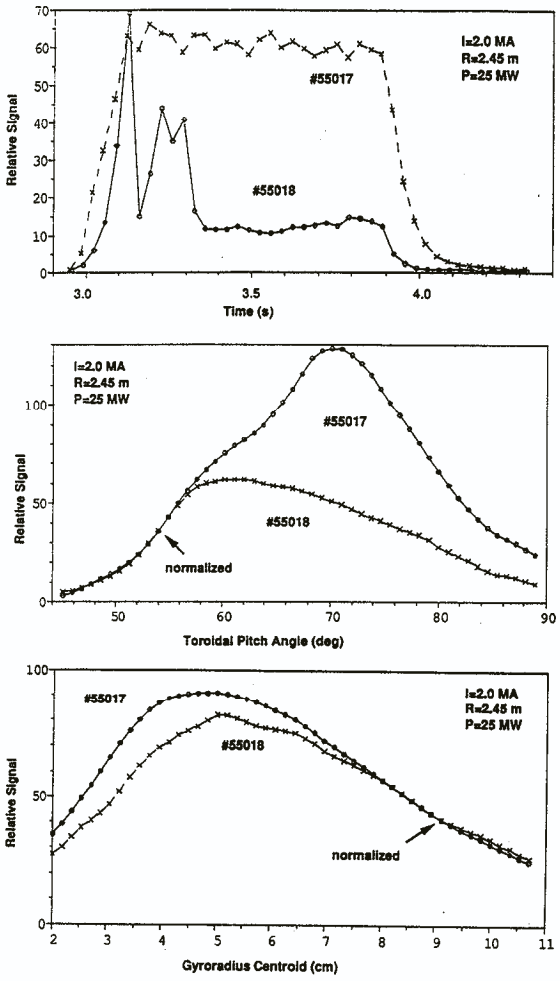

FIG. 19. Pitch angle and gyroradius distributions in a discharge without large fluctuating MHD but with a 'locked mode' apparently triggered by pre-NBI pellet injection (#55018), compared with a similar discharge (#55017) with the usual anomalous delayed loss feature (without pellets). During the time period 3.5–3.9 s the high χ, low ρ anomalous loss feature is essentially absent in #55018, as shown in the lower parts of the figure. At earlier times in the same discharge ($\approx$3.1–3.3 s) the anomalous loss feature is considerably larger than that for the discharge without large MHD (similar to Fig. 17).

camera, especially for slowly fluctuating MHD activity (e.g. with a 1 ms gate every 32 ms for Fig. 17). The time dependence of these fluctuations could be seen more clearly using a PM tube, as illustrated for a different pair of discharges in Fig. 18 (both $I = 1.75$ MA, $R = 2.45$ m and $P \approx 32$ MW). The PM signals of Fig. 18 again came from the peak loss region in the (ρ,χ) image plane, and showed a fluctuating MeV ion loss in phase with magnetic fluctuations in the case with large, slow MHD (#55 797), but not in the case with relatively less MHD activity, which had only the usual anomalous loss feature (#55 796).

An apparently different effect of MHD activity on the anomalous loss feature is illustrated in Fig. 19, which compares two discharges at $I = 2.0$ MA, $P = 25$ MW and $R = 2.45$ m (similar to that of Fig. 1). In one of these (#55 018) there was apparently a 'locked mode' during NBI, seemingly caused by an unusual sequence of pellet injection prior to NBI. In this case the anomalous loss feature near $\chi \approx 70°$ apparently *disappeared* in the 90° detector during the whole period of about 3.5–3.9 s, while the gyroradius distribution during this same period was nearly consistent with first orbit loss alone ($\rho \approx 5$–6 cm). Earlier in this same discharge there was also a period of increased loss near $\chi \approx 70°$ and $\rho \approx 3$–4 cm, similar to that shown in Fig. 17. In fact, during many discharges with large slow MHD activity (when the video camera gating time was shorter than the MHD period) the anomalous loss feature could also sometimes decrease with respect to its usual (anomalous) level without MHD activity, as shown in Fig. 17 at 3.76 s.

During the 1992 run the effects of large MHD were generally similar to those observed during the 1990 run as described above; however, one interesting result from the 1992 data is shown in Fig. 20. During one of these two $R = 2.52$ m NBI discharges (#68 522) there was a dramatic increase in the anomalous delayed loss feature about 50 ms before a major disruption, when compared with the usually small delayed loss feature in $R = 2.52$ m discharges (#69 111). This increased loss, presumably due to pre-disruptive MHD activity, occurred along with an increased loss sharply localized near the passing–trapped boundary. This shows that the delayed loss feature, which is normally small at 90° for these $R = 2.52$ m plasmas, can increase there during periods of intense MHD activity, and that MHD activity can cause both a delayed trapped particle loss and also a loss of passing particles across the passing–trapped boundary (which was probably also seen during non-disruptive MHD activity, such as in Fig. 17 at 3.89 s).

These examples show that the anomalous delayed loss feature seen in the 90° detector can be strongly modulated by MHD activity. They suggest (but do not prove) that the delayed loss normally observed without any obvious MHD activity (such as described in Sections 2.1–2.4) might be caused by some type of normally unnoticed but very reproducible internal MHD activity (or other perturbation), e.g. very slow

(< 1 Hz) or locked modes, or possibly very fast modes (f > 50 kHz). Additional data on MHD induced fusion product losses are described elsewhere [7], and theoretical mechanisms for an MHD effect are discussed in Section 3.4.1.

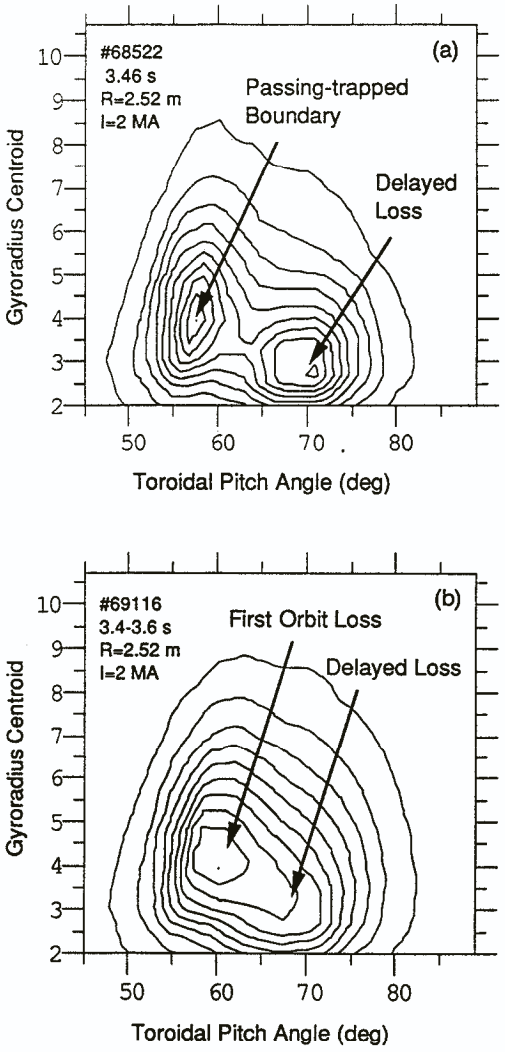

FIG. 20. Pitch angle versus gyroradius distributions for an R = 2.52 m, I = 2 MA (1992) discharge just before a major disruption (a), compared with a similar discharge without a disruption in (b). About 50 ms prior to disruption the pattern as seen in (a) shows a large delayed loss feature at a relatively high pitch angle and low gyroradius, presumably due to pre-disruptive MHD activity, along with a sharp anomalous loss feature near the passing-trapped boundary at lower pitch and higher gyroradius. The non-disruptive discharge in (b) shows comparatively less delayed loss, as is typical of large R plasmas.

3. DISCUSSION

This section discusses briefly several topics potentially relevant to an understanding of this anomalous delayed loss feature. However, these discussions should be considered preliminary, since no clear explanation for the experimental observations of Section 2 has yet been found.

3.1. Trajectories of anomalous loss orbits

The measurement of the (ρ,χ) of the lost ions at the detector allows a fairly precise calculation of the trajectory of the last orbit of the ions in the plasma. Although these orbits are useful to help determine the loss mechanism, they cannot be used to determine the previous history of the ions in the plasma.

The trajectories of three relevant loss orbits for the 90° detector are shown in Fig. 21(a), each of which has been calculated for the same plasma with R = 2.45 m and I = 2.0 MA (similar to that of Fig. 2). One of these orbits is the 'fattest banana' for first orbit loss of 3 MeV protons, which has a pitch angle of χ = 55° (see Fig. 3). This orbit trajectory misses the nearest ICRH limiter (as it was configured in 1990), and approaches within about $a/2$ of the centre of the outermost flux surface. The other two orbits are at χ = 70°, one with an assumed energy of 1 MeV and the other with 3 MeV (which bracket the range of the anomalous loss energy). These two χ = 70° orbits (and all those with intermediate energies) intersect the top of the vessel before the completion of one bounce; thus at first sight it is difficult to understand how any previously confined orbits can be lost to the 90° detector at this pitch angle in these plasmas.

One possible mechanism for this is illustrated in Fig. 21(b), which shows a typical anomalous loss orbit entering the detector at χ = 70° and E = 1.5 MeV, along with a confined orbit of the same energy which was started with an upward vertical displacement of the lower banana tip of about 15 cm with respect to the other 1.5 MeV loss orbit. The outer leg of this confined orbit just barely misses the projection of the ICRH limiter (centred at R = 2.61 m with a minor radius of 0.99 m) near the outer midplane. Thus, confined orbits with banana tips just below this one intersect the wall just below the outer midplane and not at the 90° detector location.

Therefore, the anomalous loss orbits detected at 90° could be brought there by a relatively large vertical step on the last bounce of a previously confined (and

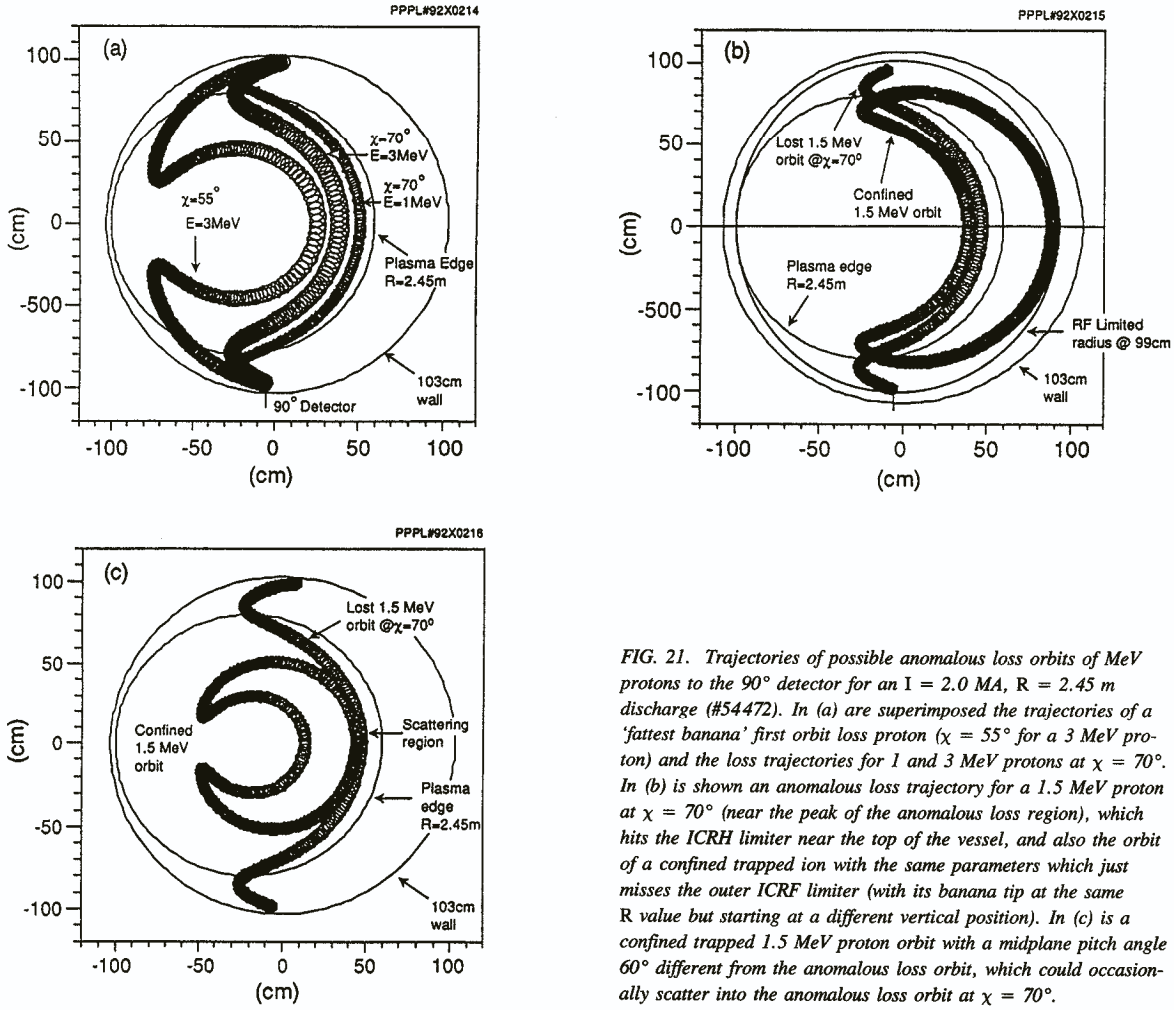

FIG. 21. Trajectories of possible anomalous loss orbits of MeV protons to the 90° detector for an I = 2.0 MA, R = 2.45 m *discharge (#54472). In (a) are superimposed the trajectories of a 'fattest banana' first orbit loss proton (χ = 55° for a 3 MeV proton) and the loss trajectories for 1 and 3 MeV protons at χ = 70°. In (b) is shown an anomalous loss trajectory for a 1.5 MeV proton at χ = 70° (near the peak of the anomalous loss region), which hits the ICRH limiter near the top of the vessel, and also the orbit of a confined trapped ion with the same parameters which just misses the outer ICRF limiter (with its banana tip at the same* R *value but starting at a different vertical position). In (c) is a confined trapped 1.5 MeV proton orbit with a midplane pitch angle 60° different from the anomalous loss orbit, which could occasionally scatter into the anomalous loss orbit at χ = 70°.*

partially thermalized) trapped orbit, while smaller vertical steps would cause the loss to occur nearer the outer midplane, as in stochastic ripple diffusion [2]. Such a large vertical step could occur while still conserving the ion's magnetic moment (banana tip major radius) and energy; some possible mechanisms for such a large last step size are discussed in Section 3.4.

Note that the real limiter and wall structure in TFTR was actually rather complicated, with two poloidal ring limiters at a minor radius of 99 cm in the 1990 run (and more at the same radius in the 1992 run), various structures at about 103 cm and a solid wall at about 116 cm. The above estimate of a step size of about 15 cm is based on numerical orbit calculations which include the two ICRF limiters at their appropriate toroidal angles for the 1990 run.

A detailed study of many such anomalous loss orbits showed that the vertical displacement of the lower banana tip required for a previously confined orbit to enter the detector aperture (for 1.5 MeV proton orbits within χ = 65–75°) was at least 10 cm, even for a single toroidally localized (but poloidally circular) limiter. The orbit–limiter intersection for these orbits occurs even for toroidally localized limiters because the co-going outer legs of these banana orbits cover a full toroidal transit within a poloidal angle range of only about ±45° from the outer equatorial midplane where $q(a) \approx 4$ (the orbit nearly follows the field line angle). Note that the effective radius of the (circular) ICRH limiter with respect to the outer leg of the banana orbit is only slightly increased over this poloidal angle range (by about 5 cm). Given the potential inaccuracies

of these orbit calculations (e.g. owing to the assumption that no current flows outside the plasma), and in the alignments of ICRH limiters (about ± 0.3 cm), it appears that a vertical step size of at least 10 cm must occur over the last bounce orbit (not necessarily at the banana tips).

The different pitch angle distributions in 1990 and 1992 (see Fig. 13) are probably caused by the differing ICRH limiter and probe geometries. In the configuration of 1990 (with the detector aperture about 4 cm below the nearest ICRH limiter 120° away toroidally) the orbits of 3 MeV protons at $I = 2$ MA calculated backward in time from the 90° detector miss the nearest limiter for all pitch angles $\chi > 30°$, whereas for the 1.5 MeV protons all the trajectories with $\chi < 55°$ hit the ICRH limiter before approaching the detector. Thus, given the uncertainty of about ± 0.3 cm in the relative positions of the detector and limiters, it is plausible that in 1990 the delayed loss orbits with low pitch angles, $\chi \approx 55$–$65°$, were shadowed by the nearest ICRH limiter. However, in the configuration of the 1992 run (with the detector aperture about 1 cm below the nearest ICRH limiter 45° away toroidally), the orbits for all 1.5 MeV (and 3 MeV) protons at $I = 1.8$ MA missed the nearest ICRH limiter for all $\chi > 45°$; thus, the low χ orbits were able to reach the 90° detector in the 1992 configuration.

In these cases the limiter shadowing effect increased for ions which stayed closer to the magnetic flux surface [5], e.g. for lower energy fusion products, but it also increases with increasing plasma current (i.e. decreasing banana width). For example, in the 1990 configuration the 3 MeV loss orbits at $I = 2.5$ MA with $\chi \leq 45°$ hit the ICRH limiter, along with 1.5 MeV orbits with $\chi \leq 59°$, which may explain the unusually low first orbit loss at this current, shown in Figs 3 and 9. Note that at the lower currents ($I \leq 1.4$ MA) all the relevant orbits easily miss the nearest ICRH limiter in both configurations, due to the large deviations of the MeV ion orbits from the flux surfaces.

The general implication of these trajectory calculations is that the poloidal, toroidal and minor radial locations of the anomalous MeV loss can depend sensitively on the relative detector and limiter positioning. This is analogous to the localization of plasma energy loss on limiter leading edges, although the large orbits of these ions can allow them to move much further into the limiter scrape-off region than the plasma itself.

3.2. Dependence on the plasma major radius

The anomalous delayed loss measured 90° below the outer midplane occurred for plasmas with major radii $R = 2.45$ m and not for plasmas with $R = 2.6$ m. For plasmas within the range $2.45 < R < 2.6$ m the anomalous feature decreased gradually towards larger R (with respect to the first orbit loss feature), and in plasmas which were moved in R during a single discharge the anomalous loss feature varied versus R in the same way as for the constant R discharges. For plasmas with smaller major radii $2.3 < R < 2.45$ m there are limited data, but the anomalous loss feature appeared to dominate at a relatively smaller plasma current than for $R = 2.45$ m plasmas (e.g. at $I = 1.4$ MA instead of $I = 1.8$ MA).

This sensitivity of the anomalous loss feature to the plasma major radius is probably due to the varying relationship between the escaping fast ions and the vessel wall, rather than to an intrinsically differing loss versus major or minor radius. Plasmas with $R = 2.6$ m are very nearly concentric with the ICRH limiter structure, so that there is very little space near the outer midplane for the outer legs of trapped ion orbits to circulate while they are moving radially (see Fig. 21). For example, in a $R = 2.6$ m plasma with $I = 2.0$ MA (in the 1990 configuration) the vertical step size needed to cause a marginally confined 1.5 MeV trapped proton orbit like that in Fig. 21(b) to hit the bottom detector at $\chi \approx 70°$ is about 25 cm, which is larger than the value of about 10–15 cm needed for the $R = 2.45$ m plasma. Thus, it is less likely that anomalous delayed loss would be detected at 90° in $R \approx 2.6$ m plasmas, assuming the same vertical step sizes for both plasmas.

In general, the poloidal intersection angle θ (below the outer midplane) of a trapped orbit which was just barely confined within the outer limiter on its last bounce is given by

$$\rho_b \{1 - [1 - (\theta/\theta_{tip})^2]^{1/2}\} - \delta r \approx \Delta R(1 - \cos\theta) \quad (1)$$

where θ_{tip} is the poloidal angle of the previously confined banana tip, ρ_b is the banana width, δr is the vertical step size of the banana tip on its last bounce and ΔR is the distance between the centre of the plasma and the centre of the (circular) wall or limiter (assuming $\Delta R \ll R$). In the limit of small δr for $\theta_{tip} \approx 1$ the solution is

$$(\theta/\theta_{tip})^2 \approx 2\delta r/(\rho_b - \Delta R)$$

which shows how the intersection angle increases as ΔR increases. Thus, for plasmas with larger R the loss should occur at smaller poloidal angles for the same vertical step size δr.

3.3. The MeV ion loss at other poloidal angles

Measurements were also made of MeV ion loss using similar detectors at poloidal angles of 60 and

45°, although the analysis is not yet as complete as for the 90° detector measurements discussed in Section 2. For the 1990 run the apertures of the 60 and 45° detectors were further outward radially than that for the 90° detector, i.e. about 6 and 8 cm behind the ICRH limiter radius, respectively (compared with about 4 cm for the 90° detector). For the 1992 run the apertures of the 60 and 45° detectors were both about 1 cm behind the shadow of the ICRH limiters (similar to the 90° detector).

For the same $R = 2.45$ m discharges which showed an anomalous delayed loss feature at 90° (i.e. with $R = 2.45$ m and $I \geq 1.4$ MA) the detectors at 60 and 45° did *not* usually show any delayed loss or distinct anomalous loss feature at high χ and low ρ, but generally had a single loss peak at a (χ,ρ) location approximately consistent with first orbit loss. However, for some plasmas with $R = 2.6$ m and $I \geq 1.4$ MA the detector at 60° showed a clear loss feature at a high pitch angle (separated from the first orbit loss at lower pitch angle), while the detector at 45° had only a single feature approximately consistent with normal first orbit loss.

This apparent absence of an anomalous delayed loss feature at poloidal angles of 60 and 45° is somewhat surprising, since it seemed from the trajectory arguments of Sections 3.1 and 3.2 that the anomalous loss feature would be larger at smaller poloidal angles (since the required vertical step size was smaller). However, it is still possible that some anomalous delayed loss was masked by the first orbit loss feature (especially if this loss was at energies nearer to the first orbit loss), or that the larger TF ripple at these smaller poloidal angles changed the character of the loss (see Section 3.4.2).

During large, slow MHD activity, such as that shown in Figs 17 and 19, there were fluctuating MHD induced increases in the signals at 60 and 45°, which were often out of phase with the increases seen in the 90° detector, as if the additional loss caused by the MHD activity was poloidally localized and rotating with the MHD mode. This suggests that the anomalous delayed loss usually seen in the 90° detector without any large MHD activity might be localized there owing to the phasing of some normally undetected locked mode in the discharge.

The movable detector at a poloidal angle of 20° showed signatures of the expected stochastic TF ripple loss for both $R = 2.6$ m and $R = 2.45$ m plasmas at $I \geq 1.0$ MA, namely, a high pitch angle feature at nearly the same gyroradius as the first orbit loss feature [2]. However, this stochastic TF ripple loss signal at $\chi \approx 60$–$65°$ could also have masked an anomalous loss signal, since the main distinguishing feature would have been a lower gyroradius component, which is not easily resolved in the present detectors. Note that the 20° detector was normally used at relatively low beam power where the anomalous loss feature was relatively small.

Again, it is important to note that these measurements of anomalous loss can be quite sensitive to radial shadowing by other limiters and even by the probe structure itself. For example, when the 20° probe was moved radially outward past the ICRH limiter radius, the size of its stochastic TF ripple loss feature (caused by an estimated radial step size per bounce of about 1 cm) decreased with respect to the first orbit loss feature [2]. Therefore, comparisons between measurements at different poloidal angles also need to take into account the potentially different effects of limiters and walls on the escaping orbit trajectories. Further analysis of the data and modelling of hypothetical anomalous loss processes will be needed to evaluate the actual poloidal distribution of the anomalous loss.

3.4. Possible causes of the anomalous delayed loss

An anomalous delayed loss of MeV ions over a timescale of $\tau_{anom} \approx 0.2$ s corresponds to an *average* anomalous diffusion coefficient of roughly $D_{anom} \approx a^2/6\tau_{anom} \approx 0.5$ m^2/s, which is much higher than the upper limit previously estimated for the diffusion of counter-passing MeV ions ($D \approx 0.1$ m^2/s) [4], which itself was larger than any collisional neoclassical diffusion rate [4]. This D_{anom} would correspond to an average radial step size per bounce of only $\delta r \approx 0.1$ cm (for a parallel length $qR \approx 1000$ cm for 1.5 MeV protons), while the trajectory calculations of Section 3.1 suggested that the last bounce has a much larger radial step size of $\delta r \approx 10$ cm. Some possible causes for this diffusion are discussed below.

3.4.1. Effects of MHD on orbit trajectories

There are two basic mechanisms by which the magnetic perturbations due to MHD activity can cause radial transport of high energy particle trajectories, namely, the parallel drift of the ion along radially perturbed field lines, and the perpendicular drifts across the field lines. The local radial drift velocity $\delta r/\delta t$ is (see Ref. [8])

$$\delta r/\delta t \approx v_{\parallel}(\tilde{B}_r/B_T) + v_{\perp} qn(\rho/r)\tilde{\delta} \qquad (2)$$

where $\tilde{B}_r$ is the local radial magnetic perturbation, q is the magnetic safety factor, n is the toroidal mode

number, ρ is the toroidal gyroradius of the fast ion and $\tilde{\delta} \approx w/R$ is the ripple amplitude induced by a flux surface displacement 'w' (the magnetic island width).

The maximum effect of the first term in Eq. (2) depends upon the maximum parallel length over which the radial perturbation points outward when followed along the fast ion orbit. To accumulate a radial step of about 10 cm over the last confined bounce period with a parallel length of $2qR \approx 1000$ cm would require that $\tilde{B}_r/B_T \approx 10^{-2}$, which appears very unlikely since the normal magnitude of internal magnetic perturbations (without large MHD) is in the range $\tilde{B}_r/B_T \approx 10^{-4}$ [7, 8]. Although a *random* radial step size implied by the latter level (about 0.1 cm per bounce) could cause a significant radial diffusion of the confined trapped ions before their last bounce, i.e.

$$D \approx (0.1 \text{ cm})^2/10^{-6} \text{ s} \approx 10^4 \text{ cm}^2/\text{s},$$

in order to cause a random step the perturbation must be above a stochastic threshold, which apparently requires $\tilde{B}_r/B_T \approx 10^{-3}$ for single mode perturbations [8, 9].

The maximum effect of the second term depends upon whether or not the orbit is near the resonant layer of the perturbation. For non-resonant orbits the effective ripple strength $\tilde{\delta}_{nr}$ is roughly $\tilde{\delta}_{nr} \approx (\tilde{B}_r/B_T)/(n - m/q)$, and so over a time of $\delta t \approx 2qR/v_\parallel$ the magnetic field perturbation needed to cause a step size of $\delta r \approx 10$ cm is again an unrealistically large $\tilde{B}_r/B_T \approx 10^{-2}$, assuming $m = 3$, $n = 1$, $q = 4$ and $v_\parallel \approx v_\perp$. However, for orbits resonant with the perturbation the effective ripple is related to the width of the local magnetic island 'w', $\tilde{\delta}_r \approx w/R \approx 4(q\tilde{B}_r/nRq'B_T)^{1/2}$. For the parameters above, a 10 cm step size would require a local $m = 3$, $q = 4$, $n = 1$ perturbation of $\tilde{B}_r/B_T \approx 6 \times 10^{-4}$, corresponding to $w \approx 10$ cm and $w/R \approx 4 \times 10^{-2}$, which is the strength of the very largest MHD perturbations in TFTR [8]. However, since the step size for resonant perturbations in Eq. (2) scales like $(n\tilde{B}_r/B_T)^{1/2}$, the step of about 10 cm could possibly be explained by an $n = 10$, $\tilde{B}_r/B_T > 2 \times 10^{-4}$ perturbation, as long as the perturbation remains in resonance with the mode (which is unlikely for a smaller scale mode like this).

Therefore, the effects of some hidden MHD activity during seemingly MHD quiescent plasmas cannot easily explain the large last step necessary to bring the escaping orbit to the 90° detector. However, MHD induced effects on confined trapped orbits might be large enough to cause the slow internal diffusion rate implied by the delayed loss. The observed modulation of the anomalous loss feature during strong MHD activity (Section 2.5) is probably due to modulation of the last vertical step, rather than variations of the internal diffusion rate.

3.4.2. *Toroidal field ripple effects*

Toroidal field (TF) ripple can act through at least two different mechanisms to cause radial transport of fast ions. The Goldston–White–Boozer (GWB) stochastic diffusion mechanism causes a collisionless radial step localized near each banana tip of [3]

$$\delta r_{GWB} \approx (N\pi/\sin\theta_b)^{1/2}(qR/r)^{3/2}\rho\delta \sin(N\varphi_b) \quad (3)$$

where N is the number of toroidal field coils ($N = 20$ in TFTR), θ_b is the poloidal angle of the banana tip ($\theta_b \approx 90°$ here), φ_b is the toroidal angle of the banana tip and δ is the TF ripple near the banana tip. For banana tips at $R \approx 2.45$ m, $z \approx \pm 80$ cm, corresponding to the orbits of Fig. 21(b), the vacuum field TF ripple is $\delta \approx 0.2$–0.3% [10], so the maximum vertical step size for 1.5 MeV protons in a 2 MA plasma at $B = 5$ T is $\delta r_{GWB} \approx 2.5$–$3.5$ cm.

Although this vertical step is apparently too small to explain the step of about 10 cm per bounce needed to cause an ion to be lost at the 90° detector (see Section 3.1), a confined trapped ion can pass through *two* banana tips before passing near the midplane (see Fig. 21(b)). Therefore, if both the top and bottom banana tips are at the proper toroidal phase angle, the net vertical step per bounce can be up to about 7 cm, which is close to the minimum needed to cause loss at 90°. However, the probability of this correlation is probably small, given the pitch angle averaging of the detectors, such that almost all of the usual GWB loss should be localized within 30° of the outer midplane, as calculated previously [2].

The other mechanism for radial fast ion transport due to TF ripple involves superbanana trapping inside the ripple wells. This mechanism could readily cause a large vertical step, although it is not clear how the orbit would be de-trapped in order to arrive at the detector with lower pitch angles such as $\chi \approx 70°$. Ripple wells occur when

$$\alpha^* = (r/R)|\sin\theta|/Nq\delta < 1 \quad (4)$$

For the banana tip location of Fig. 21(b) used above, $\alpha^* \approx 1.5$–2, which appears to be too high for ripple trapping. However, since the ripple strength δ increases rapidly nearer the edge, ripple wells are expected at $r \approx 90$ cm where $\delta \approx 0.5\%$, i.e. only about 5 cm from the lower banana tip of the 90° detector orbits of Fig. 21(b). Ripple wells occur more readily at smaller poloidal angles, e.g. over about the outer third of the

plasma minor radius at the major radius of the 60° detector.

Note that since these ripple strengths come from calculations [10] and not from actual TF measurements, it is possible that the effects of coil misalignments, small movements in situ, or stray fields from other coils might cause an increase in the GWB step size or cause the last banana tip to lie within the ripple well at the vessel bottom. However, in the absence of a detailed study of this effect, the tentative conclusion from these estimates is that TF ripple effects probably do not cause the large vertical step on the last bounce discussed in Section 3.1, although they could cause trapped orbits to diffuse radially toward that last step. However, it would be surprising if TF ripple effects alone caused the delayed loss, since, normally, fast ion orbits are either well confined or very rapidly lost owing to stochastic TF ripple diffusion [2].

3.4.3. Pitch angle scattering effects

Another conceivable mechanism for explaining the anomalous loss to the 90° detector is classical large angle scattering, which can change the pitch angle (magnetic moment) of a fast ion while changing its position by only $\approx \rho$. As shown in Fig. 21(c), a single $\approx 60°$ scattering event can cause the orbit of a confined trapped 1.5 MeV proton to be lost orbit at $\chi \approx 70°$ in the 90° detector.

The Rutherford scattering cross-section for large angle scattering of fast protons on a background hydrogenic species at an angular deflection $\geq \Phi$ is [11]: $\sigma = (\pi/4)b^2 \cot^2(\Phi/2)$, where $b = e^2/(M_0 v^2/2)$ and M_0 is the reduced mass of the colliding ions. Therefore, the characteristic rate for a 1.5 MeV proton to be scattered by $\delta\Phi \approx 60$ to 90° on background deuterons at a density of 2×10^{13} cm^{-3} is $\upsilon \approx 10^{-3}$ s^{-1}, implying that the probability of such a large angle scattering over a characteristic fast proton slowing down timescale of about 0.2 s is only $\approx 10^{-4}$. Therefore, even though the population of protons born on confined trapped orbits, such as that in Fig. 21(c), might be ten times larger than the population born on a loss orbit such as that also shown in Fig. 21(c), the large angle scattering events would cause only a small enhancement of the first orbit loss rate on this trajectory. Since the anomalous loss is larger than the expected first orbit loss on this trajectory, the process of large angle scattering cannot explain the anomalous loss. Small angle scattering is more likely; however, small angle scattering would cause a large radial step only near the passing–trapped boundary.

4. SUMMARY AND CONCLUSIONS

An anomalous loss of D–D fusion products was measured using a scintillator detector 90° below the outer midplane in TFTR. This new loss feature had a significantly lower energy than the usual first orbit loss (≈ 0.5 the birth energy), and was delayed by about 0.2 s with respect to the usual prompt first orbit loss. The orbits of the escaping ions lost in this way were fairly deeply trapped, with banana tips at about the same major radius as the plasma centre. Some observations and interpretations concerning this anomalous loss process were:

(1) The anomalous loss feature increased in strength with respect to the first orbit loss as the plasma current was increased, e.g. it was comparable with the size of the first orbit loss at $I \approx 2.0$ MA, but was negligible compared with the first orbit loss at currents $I \leq 1.0$ MA.

(2) The anomalous loss feature was visible at the 90° detector for plasmas with major radii of $R = 2.45$ m but not for plasmas with $R = 2.6$ m, possibly because the escaping ion orbits intersected the wall elsewhere for the plasmas with larger major radii.

(3) The observed delay time of about 0.2 s with respect to the prompt loss was roughly consistent with the time required for 3 MeV protons to lose about half of their energy.

(4) The strength of the anomalous loss feature increased by up to about 50% with increasing NBI power at a fixed current, suggesting that the anomalous loss was influenced by the plasma itself (even without large MHD activity).

(5) Large coherent MHD activity strongly modulated the anomalous loss feature, sometimes causing it to increase but at other times causing it to disappear, suggesting that some low level MHD activity might cause the delayed loss even in plasmas without large coherent MHD.

A rough analysis of these measurements implied that an average diffusion coefficient of $D_{anom} \approx 0.5$ m^2/s was needed to explain this loss of trapped fusion products, which is large compared with the $D < 0.1$ m^2/s previously inferred for passing fusion products [4]. This D_{anom} is comparable with the thermal plasma heat and particle diffusion coefficients, but for fusion products this corresponds to a relatively small step size per bounce of only ≈ 0.1 cm. However, a much larger vertical step size of about 10 cm on the ion's last confined bounce was required for the loss orbit to be detected at the 90° detector in the presence of the

poloidal ICRH limiters near the outer midplane. Preliminary evaluations of several possible loss mechanisms concluded that:

(a) Internal magnetic perturbations with magnitudes $\tilde{B}_r/B_T \approx 10^{-4}$ are sufficient to cause the average radial step size needed for the delayed loss, although the radial steps for single modes are apparently not stochastic below $\tilde{B}_r/B_T \approx 10^{-3}$, and even at that level a single MHD mode cannot plausibly explain the required large last step size.

(b) The calculated effect of stochastic TF ripple diffusion produced a step size of about 3 cm at each banana tip in the region of interest, and so would not quite explain the loss at 90°, although the internal radial transport of partially thermalized trapped ions could be caused by this mechanism; and localized TF ripple wells, which could cause a large vertical step size, do not quite exist in the region of the last banana tip of the anomalous loss orbit.

(c) Large angle nuclear scattering is not strong enough to cause this anomalous loss process.

Although there is as yet no quantitative explanation for the anomalous loss described in this paper, some general conclusions can be drawn from these results:

(1) This anomalous delayed loss will most likely persist for alpha particles in D–T plasmas, since they will be sensitive to similar 'single particle' loss mechanisms and will have a similar thermalization time. However, the magnitude of the global alpha heating loss will probably be <1–10% of the confined MeV ion population, corresponding to the first orbit loss level in TFTR at $I = 2$ MA [7]. Although such a loss should not affect global alpha heating, it may cause localized heat loads and damage to unprotected wall or divertor components in the ion ∇B direction.

(2) The sensitivity of these results to the radial detector relocation implies that the wall impact position of any such 'anomalous' MeV alpha loss (including that due to possible collective alpha effects) can be quite sensitive to the relative positions of the plasma, the wall and/or the limiters, and the detector itself. This suggests that MeV ion loss in future D–T experiments should ideally be monitored on all exposed limiter surfaces, although practical difficulties such as detector overheating and competing loss mechanisms will inevitably limit this information.

(3) A large guiding centre or bounce mapping code will be needed to understand the complex MHD and TF ripple loss mechanisms and their mutual interactions in the plasma; such a code should also incorporate the details of the wall and limiter geometry to determine the alpha loss locations.

Future experimental work in this area is needed to clarify the effects of the MHD mode number and its frequency on the observed anomalous loss (particularly for very low frequency modes), and should evaluate its poloidal and toroidal distributions more carefully, as done recently for NBI loss in JT-60U [12]. A search for new theoretical mechanisms for trapped fusion product loss also seems to be warranted by these results.

ACKNOWLEDGEMENTS

We thank R. Boivin, G. Hammett, M. Tuszewski and J.-P. Roubin for helpful discussions, and K. McGuire, J.D. Strachan and K.M. Young for their support of this work, which was performed under USDOE contract No. DE-AC02-76-CHO-3073.

REFERENCES

[1] ZWEBEN, S.J., et al., Nucl. Fusion **30** (1990) 1551.
[2] BOIVIN, R.L., et al., Nucl. Fusion **33** (1993) 449.
[3] GOLDSTON, R.J., et al., Phys. Rev. Lett. **47** (1983) 647.
[4] ZWEBEN, S.J., et al., Nucl. Fusion **31** (1991) 2219.
[5] ZWEBEN, S.J., et al., Rev. Sci. Instrum. **63** (1992) 564.
[6] BARNES, C.W., Los Alamos National Laboratory, personal communication, 1992.
[7] ZWEBEN, S.J., et al., IAEA-CN-56/A-6-3, paper presented at 14th Int. Conf. on Plasma Physics and Controlled Nuclear Fusion Research, Würzburg, 1992, IAEA, Vienna (in press).
[8] MYNICK, H.E., WHITE, R.B., in Theory of Fusion Plasmas (Proc. Joint Varenna–Lausanne Int. Workshop Chexbres, 1988), Editrice Compositori, Bologna (1988) 385–400.
[9] MYNICK, H.E., Transport of Energetic Ions by Low-n Magnetic Perturbations, Rep. PPPL-2856, Princeton Plasma Physics Laboratory, Princeton, New Jersey (1993).
[10] PRINCETON PLASMA PHYSICS LABORATORY, TFTR Magnetics Handbook, Doc. EAD-H-1, PPPL, Princeton, New Jersey (1983).
[11] EVANS, R.D., The Atomic Nucleus, McGraw-Hill, New York (1955) 13–16.
[12] TOBITA, K., et al., Phys. Rev. Lett. **69** (1992) 3060.

(Manuscript received 22 January 1993
Final manuscript received 11 March 1993)